3D distributions resulting from neutral beam, ICRF and EC heating in an axisymmetric mirror

R. W. Harvey' , Yu. V. Petrov' , and C. B. Forest'

Citation: **1771**, 040002 (2016); doi: 10.1063/1.4964187
View online: http://dx.doi.org/10.1063/1.4964187
View Table of Contents: http://aip.scitation.org/toc/apc/1771/1
Published by the American Institute of Physics

3D Distributions Resulting from Neutral Beam, ICRF and EC Heating in an Axisymmetric Mirror

R.W. Harvey[1, a)], Yu.V. Petrov[1, b)] and C.B. Forest[2, c)]

[1]*CompX, P.O. Box 2672, Del Mar, CA 92014, USA*
[2]*Univ. of Wisconsin, Madison, WI 53706, USA*

[a)]Corresponding author: rwharvey@compxco.com
[b)]petrov@compxco.coom
[c)]cbforest@facstaff.wisc.edu

Abstract. The CQL3D bounce-averaged Fokker-Planck (FP) code has been widely applied within the tokamak modeling community. For the reported work, it has been augmented to include axisymmetric open-field-line geometry, suitable for calculation of energetic ion and electron distributions in the low collisionality, tau_bounce << tau_collision, regime of energetic particles in mirrors. Application is made to the GDT device. Ion distributions resulting from neutral beam injected ions, in combination with quasilinear diffusion due to high harmonic fast waves are calculated. The HHFW can very efficiently enhance DD neutron production. X-mode ECH heating of electrons is modelled, giving high field first harmonic and low field second harmonic heating. The first harmonic scenario gives enhanced edge heating.

INTRODUCTION

CQL3D is a finite difference code which solves a Fokker-Planck equation in the low-collisionality regime, $\tau_{bounce} \ll \tau_{collision}$, for the time-dependent electron and ion distributions, $f_0(u_0,\theta_0,\rho;t)$ [1,2]:

$$\frac{\partial}{\partial t}(\lambda f_0) = -\nabla_{u_0}\cdot\Gamma_{u_0} + \langle\langle R\rangle\rangle + \langle\langle S\rangle\rangle, \tag{1}$$

where u_0,θ_0 are momentum-per-mass and pitch angle, and the subscript (also on f_0) indicates evaluation at the low-field point on a field line designated by flux label ρ. The distribution at other points along magnetic field B is given according to the constants of motion. The quantity $\lambda = v_{\|0}\tau_b$ is proportional to the bounce average density and enables the bounce averaged flux Γ_{u_0} to be cast in divergence form. This flux in velocity space is due to Coulomb collisions and RF quasilinear diffusion (derived from RF ray tracing data obtained with the GENRAY code[3]). The guiding center orbits for trapped particles are followed, according to the constants of motion. Perpendicular drifts are ignored. Transiting particles are taken to be rapidly lost for energies above several times the thermal value; retention of the thermal particles simulates the effects of higher collisionality of the low velocity particles. In the code runs herein, the field-line average density is maintained at given target value, by scaling the distributions at each time step; for non-isotropic distributions in pitch angle, the local density varies with distance along the magnetic surface. Self consistency is obtained between nonthermal distributions and the RF damping, by iteration. The <<*R*>> gives optional radial diffusion. <<*S*>> represents particle sources such as obtained with a Monte Carlo neutral beam (NB) deposition module. A time-implicit version of the difference equations is solved, enabling effectively rapid convergence to steady state solutions in a few time steps, or alternatively, with short time steps, enabling detailed simulation of the time-dependent distributions on collisional time-scales. The Coulomb collision operator is fully nonlinear; however, the field distribution is given as a expansion in Legendre polynomials in pitch angle, but the P_0 term is set to a Maxwellian of given density and temperature, at each time-step[1]. This is

Open Magnetic Systems for Plasma Confinement (OS2016)
AIP Conf. Proc. 1771, 040002-1–040002-5; doi: 10.1063/1.4964187
Published by AIP Publishing. 978-0-7354-1429-7/$30.00

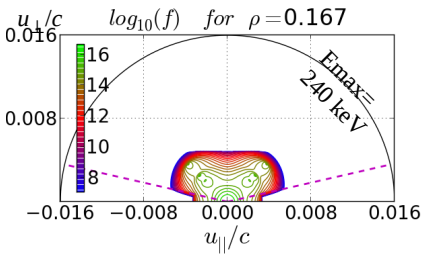

FIGURE 1. Deuterium distribution function obtained under model GDT conditions. The three NB source energies are evident.

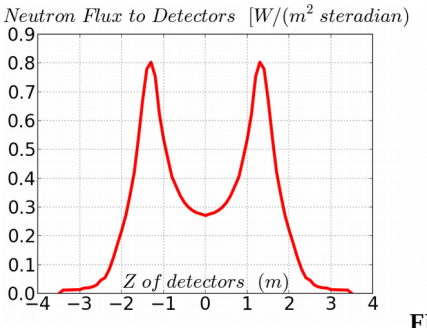

FIGURE 2. Neutron flux (W/m^2/sr) to perpendicular, central viewing detectors as a function of axial distance Z (m).

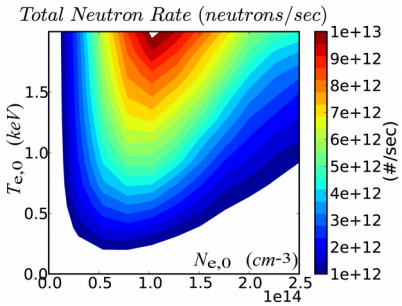

FIGURE 3. Total neutron rate from a GDT-like device, obtained as a function of central density and temperature from a set of a CQL3D simulations.

taken to simulate effects of transport and fueling, and is used to specify given "background" distribution. The CQL3D and GENRAY codes have been validated against tokamak experiments, and now have been adapted to the central cell of axisymmetric mirror geometry machines. We make initial application of the codes to the GDT environment [4,5] with NB, NB plus high harmonic fast wave (HHFW) heating or ions, and electron cyclotron resonant heating (ECRH) by high- and low-field injection.

NEUTRAL BEAM HEATING IN GDT

Figure 1 shows a deuterium distribution function at ρ=0.2 for 4 MW of 25 keV beam (also, with standard 1/2 and 1/3 energy components) injected at 45 deg into a nearly flat density N_{e0}=4.4e14/cm, peaked T_{e0}=0.6 keV GDT geometry, with mirror ratio 20. The three energies of the beam injection are evident, giving a characteristic concentration of fast ions away from the midplane as demonstrated by neutron flux to detectors placed as a function of axial length *Z*, in Fig. 2. Execution time for CQL3D is short, enabling a 121 run survey covering N_{e0}=0.8e19-20e19/m^3, T_{e0}=0.2-2.0 keV in 1 CPU hour. Total neutrons from the GDT device are given in Fig. 3. This demonstrates the approximate linear dependence of neutrons with T_{e0}, and an optimum neutron flux versus density at 1e20/m^3, above which neutral beam penetration begins to fall off. Maximum neutron rate is 1e13/sec.

NEUTRAL BEAM+HHFW HEATING IN GDT

High harmonic fast waves begin propagating at very low density near the plasma edge, and, at frequency above the ion cyclotron frequency, are accessible to arbitrarily large plasma density [6]. For a GDT device, we preliminary examine to what extent HHFW power can replace ion power, in creating a nonthermal, localized in axial length Z, distribution of hot ions and enhanced neutrons. Pitch-angle localization of fast ions due to cyclotron harmonic fast wave heating has been previously noted [7] in a manner similar to the results of oblique NBI as in Fig. 1. The

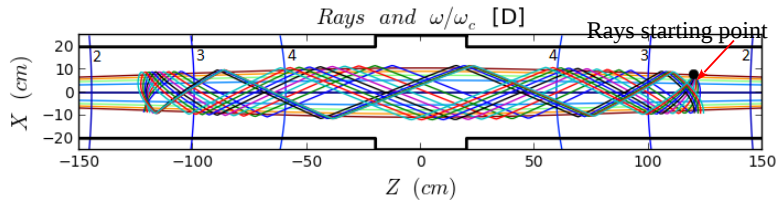

FIGURE 4. High harmonic fast wave is launched at *Z*=120 cms, frequency 11 MHz (locally between the 2nd and 3rd harmonic), into a n_{e0}=4.4e13/cc, T_{e0}=0.6 keV NB heated plasma. Self-consistent cyclotron absorption is primarily at the 3rd harmonic.

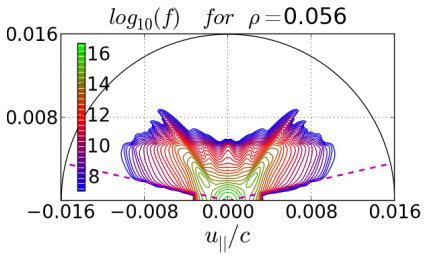

FIGURE 5. The central deuterium distribution function obtained with 4 MW of NB and 1 MW of HHFW. RF power goes 73% to ions, 24% to electrons.

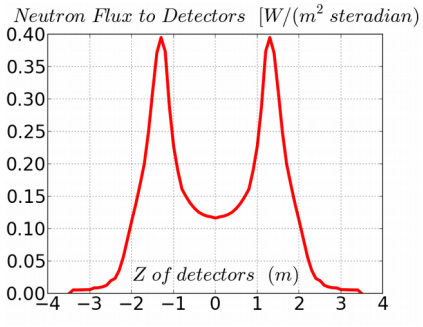

FIGURE 6. Variation of neutron flux to perpendicularly viewing detectors as a function of alias distance Z.

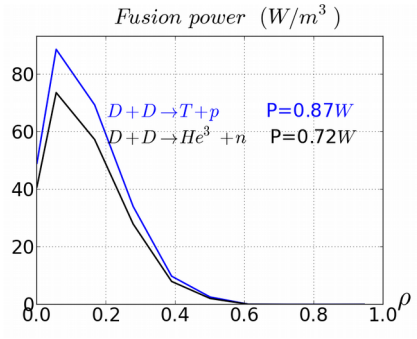

FIGURE 7. DD fusion power versus plasma radial coordinate, for the NB+ HHFW simulation. Midplane gyro-losses at the plasma edge are turned on.

NSTX spherical tokamak[8] is in a similar plasma regime as GDT. HHFW is being used on that machine to drive toroidal current by Landau damping of the HHFW, but substantial absorption on neutral beam injected ions also occurs[9,10].

For a GDT ion heating application, it appears that the HHFW must be used in conjunction with the neutral beams in order to obtain sufficient damping on ions. Compared to NB, the HHFW has an advantage for DD neutron in that it diffuses ions to very high energies, much beyond the neutral beams [2]. Figure 4 shows GENRAY ray tracing of a HHFW launched in the region of NB enhanced fast ion density near Z=125 cms. The wave frequency is chosen to be 11 MHz, intermediate between the 2nd and 3rd cyclotron harmonics, and the launched $n_{||}$ spectrum ranges in the range [-25,+25]. Those rays that start towards higher B-field are almost immediately reflected. We find that $|n_{||}|$ increases to 150 at the device midplane (Z=0) and is lower away from Z=0. Coupling the wave at such high $n_{||}$ may be difficult, in which case wave launching may be easiest at a region of B-field somewhat higher than the fast ion concentration region.

With 1MW of applied HHFW power and still 4 MW of NB, Figure 5 shows large enhancement of the tail ions beyond the neutral beam energies (compare with Fig. 1). Similar bunching up of the fast ions occurs, in Fig. 6. The DD fusion power is centrally localized (Fig. 7), but in this particular modeling the total fusion power is reduced compared to the NB only. This is due to the combined effects of our FI loss model which scrapes ions off with gyroradius greater than the plasma edge defined as ρ=1, and the RF quasilinear diffusion of fast ions into the loss cone. When FI scrapeoff losses are removed (limiter placed beyond the FI region), then the neutron power for NB only jumps up to 9.4 watts, and for NB+HHFW to 73.4 watts. That is, HHFW greatly and efficiently enhances the neutron rate.

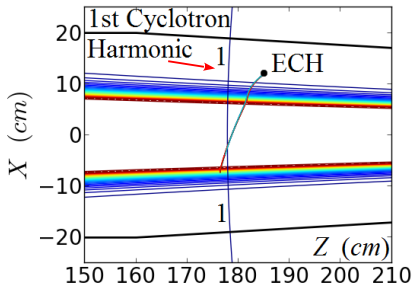

FIGURE 8. High field launch of X-mode EC waves into the plasma to fundamental resonance. Color contours represent the steep edge density rise.

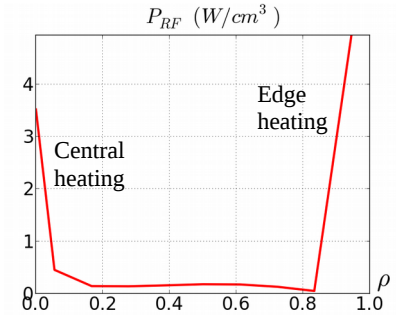

FIGURE 9. EC power deposition profile indicating sensitivity to strong edge heating, and some central heating, for high field launch.

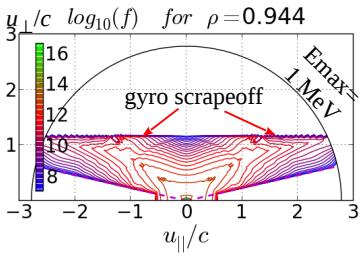

FIGURE 10. Strongly heated edge density plasma. The T_e profile ranges from T_{eo}=0.6 keV to edge value 0.1 keV. The cutoff in particles above momentum-per-mass $u_\perp/c$ =1 is due to gyroradius scrapeoff at the plasma edge.

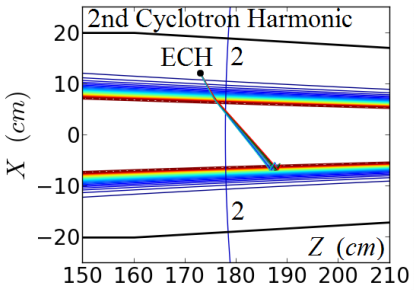

FIGURE 11. Low field X-mode EC launch towards the second harmonic. The resonance region is of restricted extent and also absorption at 2 f_{ce} is a finite-gyroradius effect.

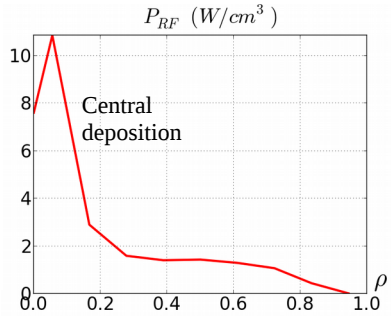

FIGURE 12. EC power deposition profile indicating well centralized heating, for high field launch.

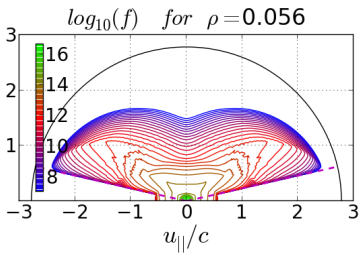

FIGURE 13. Centrally heated electron distribution, for high field X-mode launch towards second harmonic resonance.

HIGH-FIELD X-MODE 1st HARMONIC ELECTRON HEATING

Figure 8 shows launch of X-Mode waves from the high field side of the fundamental cyclotron resonance. The power deposition profile in Fig. 9 shows strong edge plasma heating. Figure 10 gives the strongly nonthermal edge electron distribution. Due to the nature of relativistic ECH heating [11], resonance exists along the rays from the plasma edge to past the resonance layer, in this case leading to large edge heating, and some focused central heating. Plasma conditions are N_{e0}=0.8e13/cc, nearly flat to edge, T_{e0}=0.6 keV, T_{eb}=0.12 keV (cf. [12]). The EC damping in the code is iterated at each time-step between the solution of the Fokker-Planck equation, and damping along the rays obtained with the quasilinear diffusion coefficients (CQL3D Manual). Thus, as a large tail electron distribution develops, the damping increases. The phenomena here may be said to be "edge blocking of the EC". It is inferred that edge heating can be an issue in similar experiments.

LOW-FIELD X-MODE 2ND HARMONIC ELECTRON HEATING

For low field second harmonic X-mode launch (Fig. 11), as is typical in tokamaks, relativistic resonance along the ray does not set in until sufficient proximity to the resonance surface is reached (depending on the $n_{||}$ value). The energy range of interaction is limited. As a consequence, strong interaction can be avoided, as in Fig. 12. The resulting strongly nonthermal central distribution is shown in Fig. 13. In both Figs. 10 and 13 scenarios, strongly nonthermal soft xray spectra are obtained.

ACKNOWLEDGMENTS

Drs. Curt Bolton, Tom Simonen, Art Molvik and Ralph Moir have been helpful and very encouraging of this work.

REFERENCES

[1] R.W. Harvey and M.G. McCoy, "The CQL3D Fokker-Planck Code" Proc. of IAEA TCM on Advances in Simulation and Modeling of Thermonuclear Plasmas, Montreal, 1992, p. 527, IAEA, Vienna (1993); Also, CQL3D Manual:www.compxco.com/cql3d_manual_150122.pdf.

[2] Yu.V Petrov and R.W. Harvey, "A Fully-Neoclassical Finite-Orbit-Width Version of the CQL3D Fokker-Planck code", submitted for publication (2016). Also, see www.compxco.com/cql3d.html.

[3] A.P. Smirnov and R.W. Harvey, The GENRAY Ray Tracing Code, CompX report CompX-2000-01 (2001). Also, see www.compxco.com/genray.html.

[4] Mirnov, V. V., Riutov, D. D., "Linear gasdynamic system for plasma confinement", (Pisma v Zhurnal Tekhnischeskoi Fiziki, vol. 5, June 12, 1979) Soviet Technical Physics Letters, vol. **5**, 279 (1979).

[5] A.A. Ivanov and V.V. Prikhodko, Plasma Phys. And Controlled Fusion 55, 063001 (2013).
[6] S.C. Chiu, V.S. Chan, R.W. Harvey, M. Porkolab, Nucl. Fus. **29**, 2175 (1989).
[7] R.W. Harvey, M.G. McCoy, G.D. Kerbel, Nucl. Fus. 26, 43 (1986).
[8] M. Ono, S.M. Kaye, Y.-K.M. Peng et al., Nucl. Fusion **40**, 557 (2000).
[9] A.L. Rosenberg, J.E. Menard, et al., Phys. of Fluids **11**, 2441 (2004).
[10] R.W. Harvey, Yu.V. Petrov, D. Liu, W.W. Heidbrink, G. Taylor, P.T. Bonoli, "CQL3D-HYBRID-FOW Modeling of the Temporal Dynamics of NSTX NBI+HHFW Discharges", Proc. of the 20th Topical Conf. on Radio Frequency Power in Plasmas, Sorrento, Italy, June 25-28 (2013).
[11] R.W. Harvey, M.G. McCoy and G.D. Kerbel, Phys. Rev. Lett. **62**, 426 (1989).
[12] P.A. Bagryansky, A.G. Shalashov, E.D. Gospodchikov, et al., Phys. Rev. Lett. 205001 (2015).